RSC Advances

PAPER

View Article Online
View Journal | View Issue

Cite this: *RSC Adv.*, 2015, **5**, 30841

Ag-modified AgI–TiO_2 as an excellent and durable catalyst for catalytic oxidation of elemental mercury

Songjian Zhao, Zan Qu,* Naiqiang Yan,* Zhen Li, Wenfei Zhu, Jie pan, Jianfang Xu and Mengdan Li

Received 15th January 2015
Accepted 16th March 2015

DOI: 10.1039/c5ra00838g

www.rsc.org/advances

AgI–TiO_2 was employed for the removal of elemental mercury (Hg^0) from flue gas, and extra elemental silver (Ag) was introduced to enhance the catalytic activity and stability. AgI–TiO_2 displayed an excellent effect on Hg^0 catalytic oxidation, and the Hg^0 oxidation efficiency was almost 100% with only 5 ppm HCl at 350 °C, which was better than that of KI–Ti. Adding Ag to AgI–TiO_2 can notably prolong the period of high efficiency, and the Hg^0 oxidation efficiency was still above 90% after 10 h with only 2% Ag added. Doping with silver could suppress the decomposition of AgI and the loss of iodine, which maintains the stability of the catalyst performance. In addition, HCl was readily adsorbed and activated by the silver. The iodine in Ag(2%)–AgI–Ti mainly acted as an accelerant for Hg^0 oxidation by facilitating formation of the intermediate Hg–I*; then, chlorine can further convert the intermediate to $HgCl_2$ as the final product. In addition, the thermogravimetric (TG) analysis proved that Ag(2%)–AgI–Ti showed a good stability at high temperature. Furthermore, the ion chromatogram tests also showed the chemical stability of AgI–Ti in the presence of Ag.

Introduction

The emission of mercury from coal-fired power plants has attracted increasing concern in recent years because of its high toxicity, volatility and bioaccumulation.[1] The Minamata Convention on Mercury, which was signed by most countries in October 2013, will be put into force to prevent Hg emission worldwide.[2,3] As one of the largest mercury emission countries, China has also paid increasing attention to mercury control, and the government has issued the "Emission Standard of Air Pollutants for Thermal Power Plants" (GB13223-2011) to reduce mercury emissions, which was implemented in January 2015.[4]

Generally, mercury exists in three forms in coal-fired flue gas: elemental (Hg^0), oxidized (Hg^{2+}), and particle-bound (Hg^p).[5] Hg^{2+} and Hg^p are relatively readily removed from flue gas by using typical air pollution control devices, such as ESPs and wet-FGD.[6] However, Hg^0 is difficult to remove from flue gas due to its high volatility and low solubility in water.[7] The technologies for the abatement of Hg^0 mainly focus on two methods: enhanced adsorption or oxidation. The adsorption processes, such as halide-modified activated carbon injection, are expensive and may cause secondary environmental problems.[8,9] Consequently, the catalytic oxidation process is a promising choice, and the generated Hg^{2+} can be subsequently captured by the existing air pollution control devices.

It is reported that HCl is an important species that affects mercury oxidation, because the major oxidized mercury species in coal-fired flue gas is $HgCl_2$.[10] Other halogen species can also oxidize Hg^0, such as bromine[11,12] and iodine, of which iodine was found to be the most efficient oxidant.[13] In addition, HCl can react with HI or I_2 to generate an interhalogen species (ICl), which is a very efficient oxidant for Hg^0 oxidation.[13,14] However, iodine release might bring unexpected pollution problems if too much iodine is used in flue gas, and I_2 sublimates at a relatively low temperature.

Silver has been recognized as an active catalytic element and has subsequently been used in various catalysts.[7,15] Ag has also been used for adsorbent materials to remove Hg^0 at low temperatures through an amalgamation mechanism. In addition, Ag can generate electrophilic oxygen, which is beneficial for the reaction. The combination of silver and iodine might enhance the efficiency of Hg^0 oxidation.

In addition, AgI is also a very important catalyst, extensively used in the fields of photography and photocatalysis. However, AgI is unstable due to the fact that it can decompose into Ag when exposed to light. Many studies have shown that metallic silver species present on the surface are able to inhibit the decomposition of AgX, so adding silver could enhance the catalytic activity and stability.[16,17] Furthermore, it has been found that AgI can maintain its stability when loaded on a semiconductor support such as TiO_2.[18] Therefore, Ag-modified

School of Environmental Science and Engineering, Shanghai Jiao Tong University, 800 Dong Chuan Road, Shanghai, 200240, PR China. E-mail: quzan@sjtu.edu.cn; nqyan@sjtu.edu.cn; Tel: +86 21 54745591

AgI–TiO_2 might be used for catalytic oxidation of elemental mercury. However, no report regarding an Ag-modified AgI–TiO_2 catalyst for Hg^0 removal has been found as yet.

In the present study, catalysts were prepared using a room-temperature impregnation method. The physical and chemical properties of the catalysts, as well as the Hg^0 oxidation efficiency of the Ag-modified AgI–TiO_2 catalyst at low HCl concentrations, were investigated. Furthermore, the catalytic mechanism involved in improving the efficiency was discussed.

Experimental section

Sample preparation

Catalysts were prepared using the impregnation method and included KI–TiO_2, AgI–TiO_2, and Ag–AgI–TiO_2. For the preparation of KI–TiO_2, an appropriate amount of TiO_2 powder (Degussa P25) and KI were mixed by stirring for 1 h, and this mixture was marked as solution A. Then, solution A was dried with a rotary evaporation apparatus, and finally calcined in a muffle furnace (5 h, 500 °C). For AgI–TiO_2 and Ag–AgI–TiO_2, PVP and $AgNO_3$ precursor were mixed and stirred for 6 h at room temperature; this mixture was added dropwise into solution A and stirred constantly for 2 h, then the mixed solution was dried and calcined as above. The difference between AgI–TiO_2 and Ag–AgI–TiO_2 was that the stoichiometry of Ag to iodide was more than 1.0 for the latter. The KI–TiO_2, Ag–TiO_2 and Ag–AgI–TiO_2 catalysts were labeled as KI–Ti, Ag–Ti and Ag–AgI–Ti. The elemental ratio of Ag or I to TiO_2 is on the basis of the atom percentages, such that Ag(x%)–Ti represents the Ag/TiO_2 mole ratio, and the elemental ratio (1%) was omitted.

Catalytic activity evaluation

The catalytic activity evaluation of the catalysts was similar to that described previously.[7] It consisted of a simulated gas preparation system, catalytic reaction device, cold vapor atomic absorption spectrometer (CVAAS) and an online data acquisition system. Hg^0 vapor was prepared from the Hg^0 permeation unit and was blended with the gases before entering the reactor. The concentration of elemental mercury in the gas was analyzed using a mercury analyzer (CVAAS SG-921). The gas containing the elemental mercury was firstly passed through the bypass and then sent to the CVAAS to determine the baseline. When the concentration of elemental mercury fluctuated within ±5% for more than 30 min, the gas was shifted to the catalytic reactor containing the catalyst. When the catalyst was saturated with Hg^0, 5 ppm HCl was passed through to estimate the Hg^0 oxidation efficiency. Because the catalysts were first saturated with about 300 μg m^{-3} of Hg^0 with N_2 and O_2 gas flow, the decrease in Hg^0 concentration across the catalyst after passing through HCl was attributed to Hg^0 oxidation. Therefore, the definition of Hg^0 oxidation efficiency (E_{oxi}) over the catalyst is as follows:

$$E_{oxi}(\%) = \frac{\Delta Hg^0}{Hg^0_{in}} = \frac{Hg^0_{in} - Hg^0_{out}}{Hg^0_{in}}$$

The gas flow rate corresponded to a space velocity (SV) of 4.26 × 10^5 h^{-1}. Nitrogen was used as the carrier gas, and the oxygen content was set at 4%.

Characterization of the catalysts

Powder X-ray diffraction patterns were recorded between 10° and 80° at a step of 7° min^{-1} on an X-ray diffractometer (APLX-DUO, BRUKER, Germany) using Cu Kα radiation (40 kv and 20 mA). The microstructure of the catalysts was analyzed using transmission electron microscopy (TEM). Samples were dispersed in ethanol with strong sonication before analysis. Hydrogen temperature program reduction (H_2-TPR) experiments were performed on a Chemisorp TPx 2920 instrument; the catalysts were degassed at 200 °C for 3 h under Ar atmosphere before the H_2-TPR test, and the reducing gas was 10% H_2/Ar. The X-ray photoelectron spectroscopy (XPS) measurements were carried out with an AXIS UItraDLD (Shimadzu-Kratos) spectrometer with Al Kα as the excitation source. The C 1s line at 284.8 ev was taken as a reference for the binding energy calibration. The reaction when passing through 5000 ppm HCl was monitored *in situ* using a UV/vis spectrometer (BDS130, USA) equipped with an optical fiber for UV-beam transmission and a detector in the range of 200–800 nm. The maxima of UV adsorption for iodine, iodine monochloride and chlorine were around the wavelengths of 530 nm, 467 nm and 330 nm, respectively.[19] The reaction products were dissolved in ultrapure water and analyzed by ion chromatography (BP-100). The thermal stability of the catalysts was determined using a TGA/DSC1 (Mettler Toledo); N_2 was used as the carrier gas, and the heating rate was 5 °C min^{-1}. Hg^0 adsorption experiments were conducted by passing flue gas containing Hg^0, N_2 and 4% O_2 over the prepared catalyst, and recording the Hg^0 signal curve. Measurement of the temperature programmed desorption (TPD) curves of Hg^0 proceeded as follows: an appropriate amount of catalyst was placed in a fixed-bed reactor with N_2 + 4% O_2 at 30 L h^{-1} and 100 °C to adsorb mercury for 2 h; afterwards, the oxygen was stopped, and the Hg^0 signal curve was recorded at 2 °C min^{-1} up to 450 °C, under nitrogen.

Results and discussion

Comparison of the Hg^0 catalytic oxidation efficiencies of various catalysts

Fig. 1 shows the comparison of the Hg^0 catalytic oxidation efficiencies over various catalysts at 350 °C. The Hg^0 oxidation efficiency of AgI–Ti was higher than that of KI–Ti, which indicated that for AgI–Ti there were more active species to oxidize Hg^0 after HCl was passed through. However, the Hg^0 oxidation efficiency decreased with time, suggesting that the performance of AgI–Ti was unstable. When silver was added, the high-efficiency period was obviously prolonged. However, the efficiency declined for high silver content, which might be due to the fact that a high content of silver inhibited the catalysis of AgI. Therefore, 2% Ag content was suitable. The Hg^0 oxidation efficiency was still above 90% after 10 h, indicating that Ag(2%)–AgI–Ti was a high-performance catalyst for Hg^0 catalytic

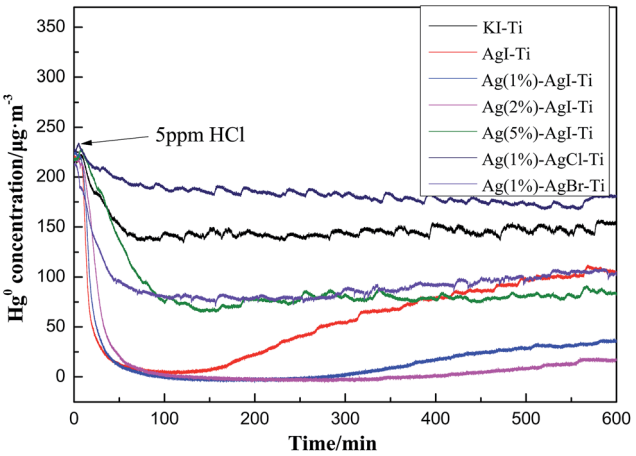

Fig. 1 The comparison of the Hg^0 catalytic oxidation efficiencies over various catalysts at 350 °C.

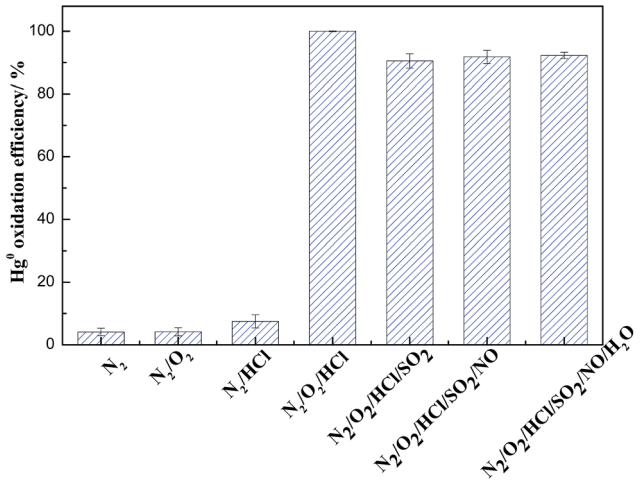

Fig. 3 The Hg^0 catalytic oxidation efficiencies of Ag(2%)–AgI–Ti under various conditions.

oxidation. In addition, the Hg^0 catalytic performance of Ag(1%)–AgI–Ti was better than those of Ag(1%)–AgCl–Ti and Ag(1%)–AgBr–Ti, demonstrating that iodine was the most efficient for Hg^0 oxidation among the halogen species. Therefore, the physical and chemical properties of the catalysts and the reaction mechanism needed to be studied.

Catalyst activity

Fig. 2 shows the Hg^0 oxidation efficiencies over Ag(2%)–AgI–Ti at various temperatures after passing through 5 ppm HCl. As can be seen from Fig. 2, the catalytic efficiency of Ag(2%)–AgI–Ti was improved with increasing temperature, and the Hg^0 oxidation efficiency could reach 100% above 350 °C. This indicated that the suitable reaction temperature for oxidizing Hg^0 was at high temperature, and there were more active species to oxidize Hg^0 at high temperature.

The Hg^0 catalytic oxidation efficiencies of Ag(2%)–AgI–Ti under various conditions are shown in Fig. 3. Ag(2%)–AgI–Ti had little catalytic ability with only O_2 or HCl. When O_2 and HCl were both present, the oxidation efficiency was high, demonstrating that HCl was the main catalytic component. Active Cl or Cl_2 would be generated by the catalysis of Ag(2%)–AgI–Ti in the presence of O_2, which could react with AgI to produce ICl or I_2 to oxidize Hg^0. When 500 ppm SO_2 was passed through, the performance of the catalyst was slightly inhibited, which might be due to the fact that some of the active Cl would react with SO_2.[13] The efficiency improved slightly when adding 500 ppm NO, indicating that NO promoted the Hg^0 oxidation.[20] In addition, 4% H_2O had little effect on the Hg^0 oxidation.

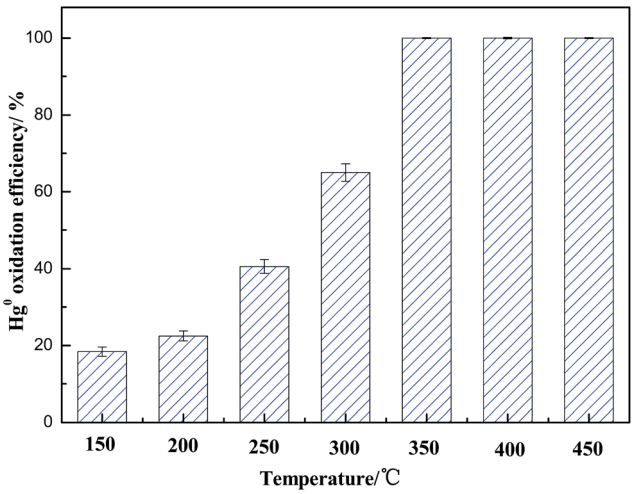

Fig. 2 The Hg^0 oxidation efficiencies over Ag(2%)–AgI–Ti at various temperatures after passing 5 ppm HCl.

Microstructural characterizations

To obtain information on the microscopic morphologies, transmission electron microscopy (TEM) analyses of the AgI–Ti and Ag(2%)–AgI–Ti nanoparticles were carried out, as shown in Fig. 4. The AgI–Ti catalyst was made up of nanoparticles and the sizes were between 20 and 40 nm, as shown in Fig. 4(a). The elemental composition of AgI–Ti according to the EDS analysis (Table 1) proves the existence of AgI on the carrier. In addition, the HRTEM image in Fig. 4(b) corresponding to the circled part in Fig. 4(a) shows crystal lattices with distances of 0.23 nm and 0.35 nm, which can be attributed to the (110) plane of β-AgI and the (101) plane of anatase TiO_2, respectively, further proving the existence of AgI on the TiO_2.[21,22] In contrast with Fig. 4(a), there were many small particles attached on the surfaces of the TiO_2 in Fig. 4(c), which were Ag nanoparticles. The AgI nanoparticles were also found in the HRTEM image in Fig. 4(d), corresponding to the circled part in Fig. 4(c). In addition, the content of iodine for Ag(2%)–AgI–Ti was higher than that of AgI–Ti according to the results in Table 1. This indicated that the catalyst was prepared successfully and adding the silver could efficiently inhibit the decomposition of AgI.

X-ray diffraction study

Fig. 5 shows the XRD patterns of the various catalysts calcined at 500 °C. The anatase and the rutile phases of TiO_2 can be seen

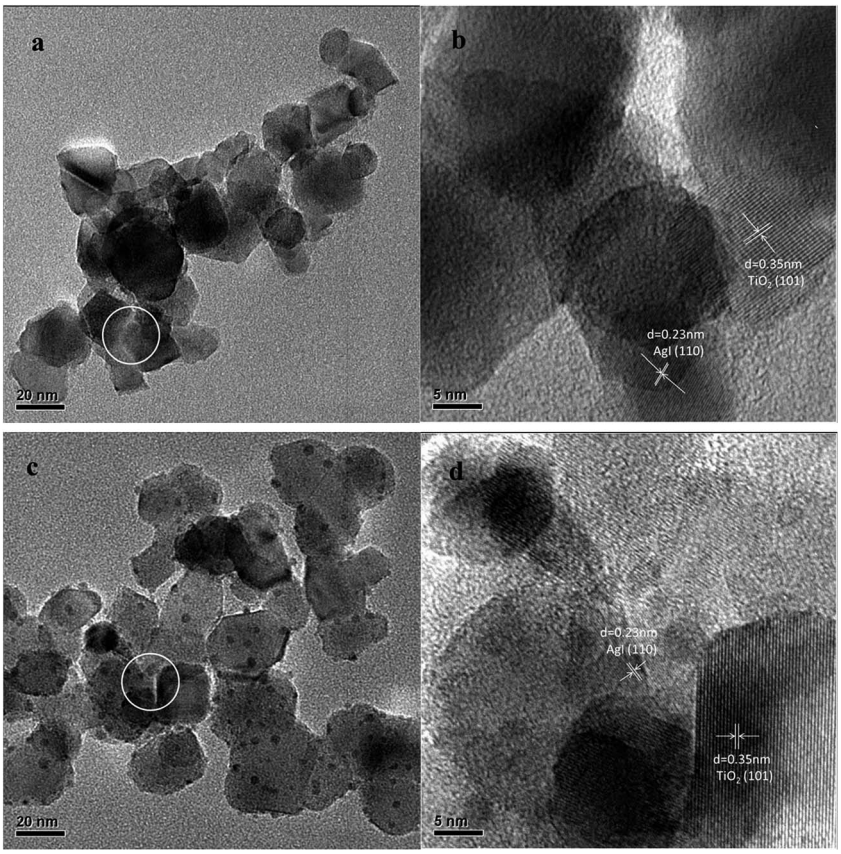

Fig. 4 TEM and HRTEM images: AgI–Ti (a and b) and Ag(2%)–AgI–Ti (c and d).

Table 1 The elemental composition of AgI–Ti and Ag(2%)–AgI–Ti according to EDS analysis

	Element	Weight%	Atomic%
Ag(2%)–AgI–Ti	O K	44.69	71.96
	Ti K	49.77	26.77
	Ag L	4.27	1.02
	I L	1.26	0.26
AgI–Ti	O K	83.36	94.24
	Ti K	14.17	5.35
	Ag L	2.08	0.35
	I L	0.39	0.06
	Totals	100.00	

for all catalysts in Fig. 5. The peak at 32.8 ev was indexed to the (102) planes of the hexagonal β-AgI crystal phase,[16] which was weak in Fig. 5(b)–(d) due to the low content. Additionally, no noticeable silver oxide and metal peaks were observed in the X-ray diffractograms in Fig. 5(b) and (c), because the amount of Ag dopant was low or the strongest Ag peak (111) was overlapped with that of anatase (004). The Ag^0 characteristic peaks could be observed in Fig. 5(d), indicating that the added silver was loaded on the support in the metallic state.

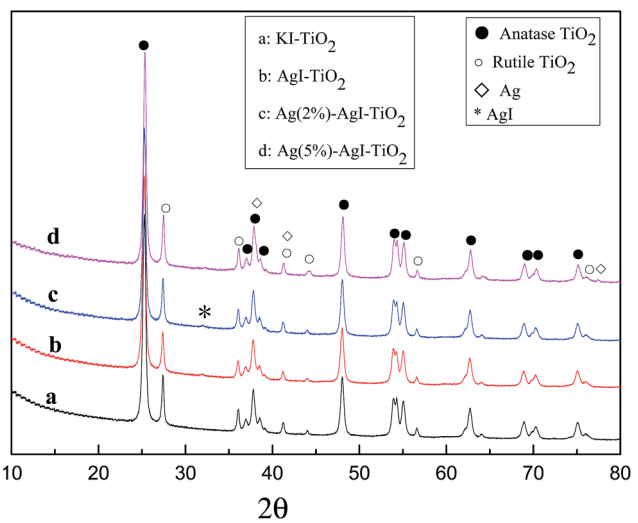

Fig. 5 The XRD patterns of the various catalysts calcined at 500 °C.

XPS analysis

Fig. 6 shows the XPS spectra of AgI–Ti and Ag(2%)–AgI–Ti over the spectral regions of Ag 3d, I 3d, O 1s, Ti 2p, Cl 2p and Hg 2p. The spectra of I 3d in Fig. 6(a) show that the binding energies of I 3d5/2 and I 3d3/2 were located at about 630.5 eV and 618.5 eV, respectively, which could be ascribed to the I^- in AgI.[23,24] The I 3d peaks of Ag(2%)–AgI–Ti were enhanced compared with those of AgI–Ti, suggesting that the content of iodine was higher for Ag(2%)–AgI–Ti. This indicated that the addition of silver could

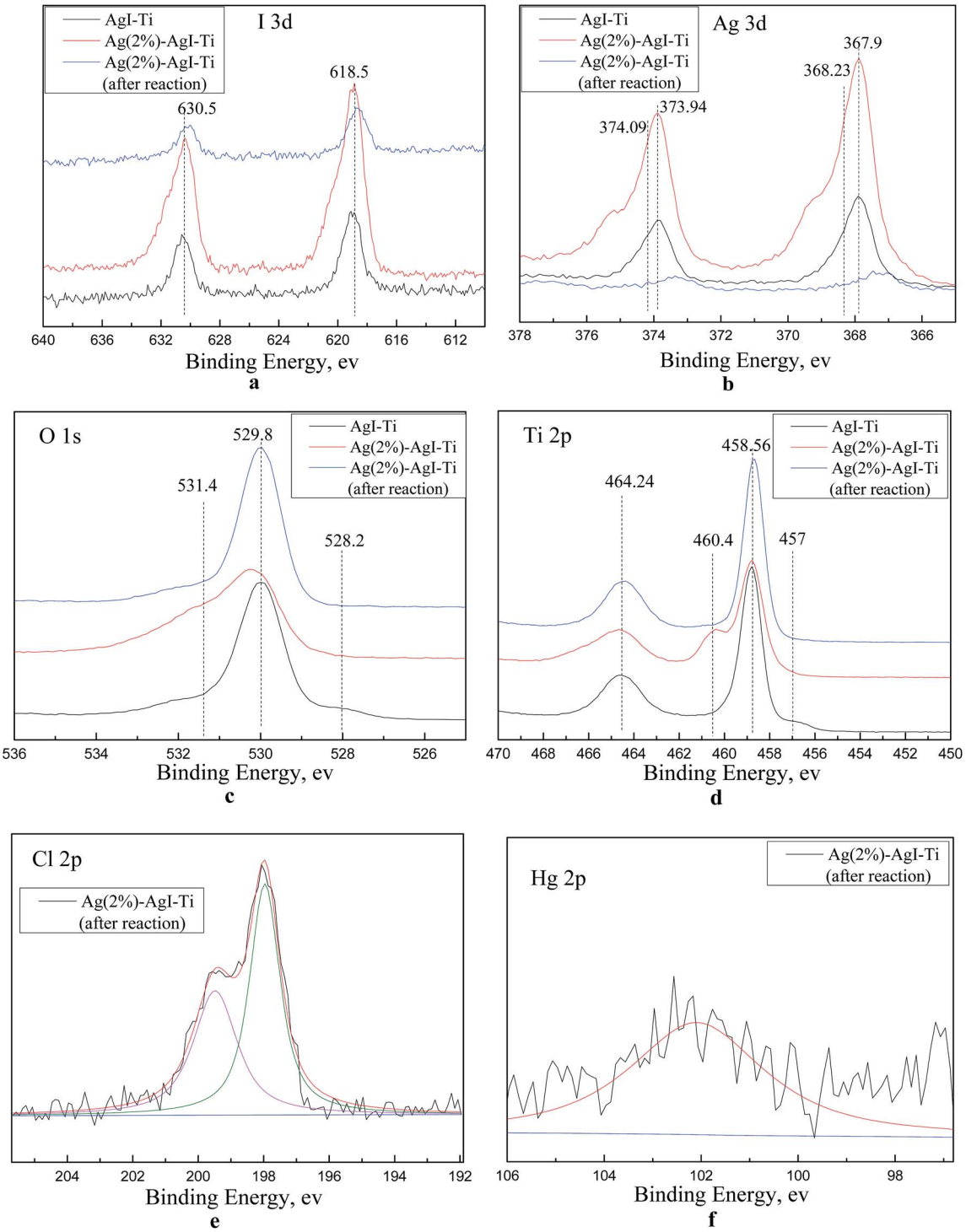

Fig. 6 The XPS spectra of AgI–Ti and Ag(2%)–AgI–Ti over the following spectral regions: I 3d (a), Ag 3d (b), O 1s (c), Ti 2p (d), Cl 2p (e) and Hg 2p (f).

maintain the stability of AgI and was beneficial for the catalytic reaction. After passing through HCl, the strength of the I 3d peaks was reduced, which might be due to the fact that Hg^0 or Cl species were adsorbed on the surface of iodine.

Fig. 6(b) shows the XPS peaks of Ag 3d. It was reported that the peaks at 367.90 eV and 373.94 eV are attributed to Ag (I), and those at 368.23 eV and 374.09 eV are attributed to metallic silver, Ag (0).[21] It could be found that the silver nanoparticles were present as a mixture of metallic silver (Ag^0) and Ag^+ (AgI) for AgI–Ti and Ag(2%)–AgI–Ti, in which the Ag^+ was dominant, demonstrating the existence of AgI, and it could also be concluded that some of the AgI was decomposed to Ag^0. By

adding silver to AgI–Ti, the greater content of metallic silver could stabilize AgI, so that the Ag^+ peak intensity of Ag(2%)–AgI–Ti was increased. After passing through HCl, the intensity of the characteristic peaks was weakened. This might be because HCl or Cl was adsorbed on the surface of the Ag. The characteristic peak of silver was shifted to low binding energy due to the effect of HCl.

The O 1s XPS spectrum is shown in Fig. 6(c). The peak at 529.8 eV might be ascribed to lattice oxygen, and the peak at 531.4 eV could be attributed to surface chemisorbed oxygen. In addition, the peak at 528.2 eV corresponded to nucleophilic states and that at 530.4 eV denoted electrophilic states for the O 1s, and the electrophilic oxygen was beneficial for the oxidation reaction.[7] It could be found from Fig. 6(c) that there was no nucleophilic oxygen after adding silver, and the chemisorbed oxygen and electrophilic oxygen were present, which was beneficial for the oxidation ability of the catalyst. When the HCl was passed through, the surface chemisorbed oxygen decreased, suggesting that HCl and oxygen were activated by the silver and reacted with each other. The reaction path might be that an electron of HCl was transferred by silver to the chemisorbed oxygen. Active chlorine was produced and then I^- or Hg^0 was oxidized, and the generated oxygen anion combined with hydrogen ions into water.[17]

The two typical Ti 2p peaks located at approximately 458.56 eV and 464.24 eV can be assigned to Ti^{4+} 2p3/2 and Ti^{4+} 2p1/2, respectively, in Fig. 6(d).[25] An additional peak at 457 eV for AgI–Ti in Fig. 6(d) was detected that matched the trivalent state of titanium,[25] which disappears for Ag(2%)–AgI–Ti. An obvious shoulder at about 460.4 ev was also attributed to Ti^{4+} 2p3/2,[26] as shown in Fig. 6(d). This indicated that the surface-deposited Ag could induce a change in the Ti chemical states, maintaining the higher oxidation states of Ti.

The Cl 2p XPS spectrum is shown in Fig. 6(e). There are two peaks at 197.8 and 199.7 eV for Cl 2p, which are attributable to ionic (Cl^-) and covalent (–Cl) chlorine species, respectively.[27] The ionic chlorine (Cl^-) might be the $HgCl_2$ generated by the reaction of chlorine species and mercury or chlorine species and HgI_2.[19] The covalent (–Cl) chlorine species might be the adsorbed HCl or generated ICl.

The Hg 4f XPS patterns are shown in Fig. 6(f). It was found that the peak of Hg 4f was at about 101.8 eV, which was significantly higher than the binding energy of Hg^0 (99.9 eV).[28] This inferred that there was no Hg^0 on the surface of catalyst. Tao *et al.* reported that the binding energies for Hg 4f 5/2 and Hg 4f 7/2 can be attributed to HgO (with the peak at 104.4 eV) and $HgCl_2$ (101.4 eV).[29] The Hg 4f peak in Fig. 6(f) could be Hg^{2+}, indicating that Hg^0 was oxidized by the catalyst. In addition, the peak intensity of Hg 4f peak was weak, which suggested that the reaction product was adsorbed less on the surface of catalyst, and most of the mercury oxidation occurred in the gas.

TPR analysis

The TPR profiles of the various catalysts are shown in Fig. 7. As can be seen in Fig. 7, P25 has no obvious peak, and the oxidation ability was weak. There was a peak at about 600 °C for KI–Ti, showing that the catalyst started to decompose to form I_2 at this temperature. In addition, it can be seen clearly that the oxidation ability of AgI–Ti and Ag(2%)–AgI–Ti was higher than that of KI–Ti and the catalytic performance was stable. The peak at 180 °C was stronger for Ag(2%)–AgI–Ti, which might be due to the larger proportion of Ag^0, facilitating production of active hydrogen and hydrogen overflow, or due to Ag_2O.[7,30] As can be also seen that the performance of Ag(2%)–AgI–Ti was more stable with the increase in temperature than that of AgI–Ti, indicating the important role of silver.

The analysis of the catalytic mechanism

The analysis of the mercury combination property. In order to study the mercury combination property of the catalysts, Hg^0 adsorption and desorption experiments were performed. Fig. 8(a) shows the Hg^0 breakthrough curves over Ag(2%)–AgI–Ti at various temperatures. As can be seen from Fig. 8(a), the adsorption ability of Hg^0 was poor above 300 °C, indicating that Hg^0 was hardly adsorbed at high temperature. In addition, AgI was stable and not decomposed below 400 °C. The Hg^0 concentration was reduced slightly at 450 °C, which might be due to the generated active I, which oxidized Hg^0. The Hg^0 concentration is still high, indicating that the amount of active I was less and AgI was still stable.

The Hg-TPD curve for Ag(2%)–AgI–Ti is shown in Fig. 8(b). It can be seen from Fig. 8(b) that some amount of Hg^0 was desorbed at low temperature, which might be the decomposition of the silver amalgam. There was little desorbed Hg^0 above 300 °C, indicating that Hg^0 was hardly adsorbed on the surface of the catalyst at high temperature, in accordance with the results of Fig. 8(a). The Hg^0 concentration decreased at 450 °C, which might be due to the small amounts of active I generated.

The analysis of the UV/vis spectrum. In order to probe the role of HCl for Hg^0 oxidation, the reaction when passing HCl over Ag(2%)–AgI–Ti was recorded using a UV/vis spectrometer. There were no obvious characteristic peaks for Ag(2%)–AgI–Ti

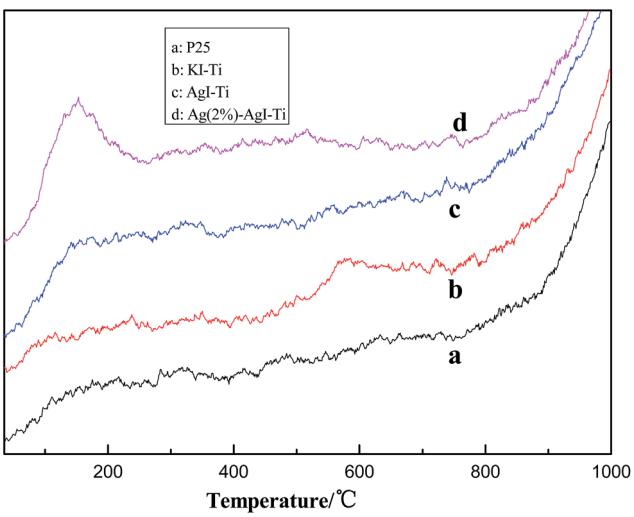

Fig. 7 TPR profiles of the various catalysts: P25 (a), KI–Ti (b), AgI–Ti (c), Ag(2%)–AgI–Ti (d).

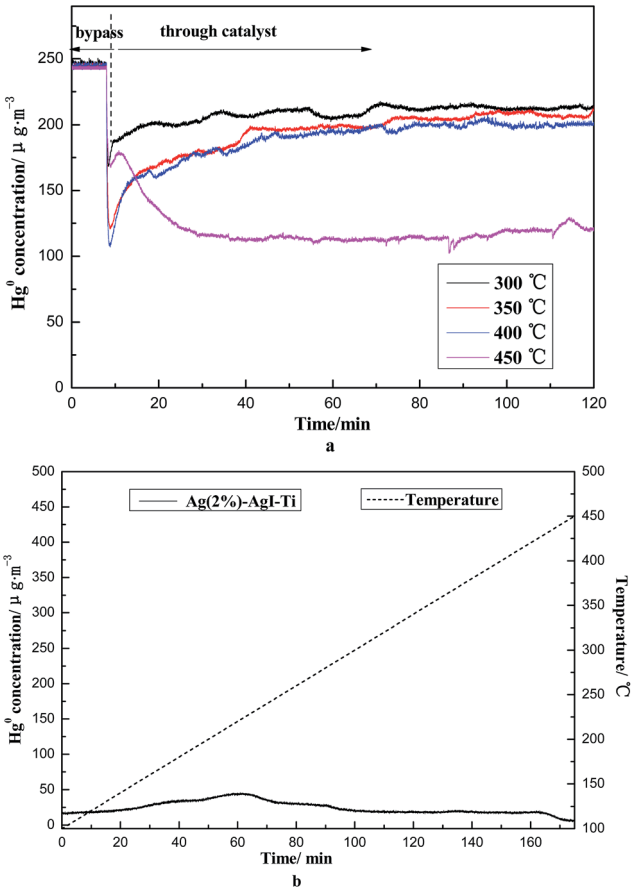

Fig. 8 The Hg^0 adsorption and desorption curves over Ag(2%)–AgI–Ti: the Hg^0 breakthrough curves at various temperatures (a), the Hg-TPD curve (b).

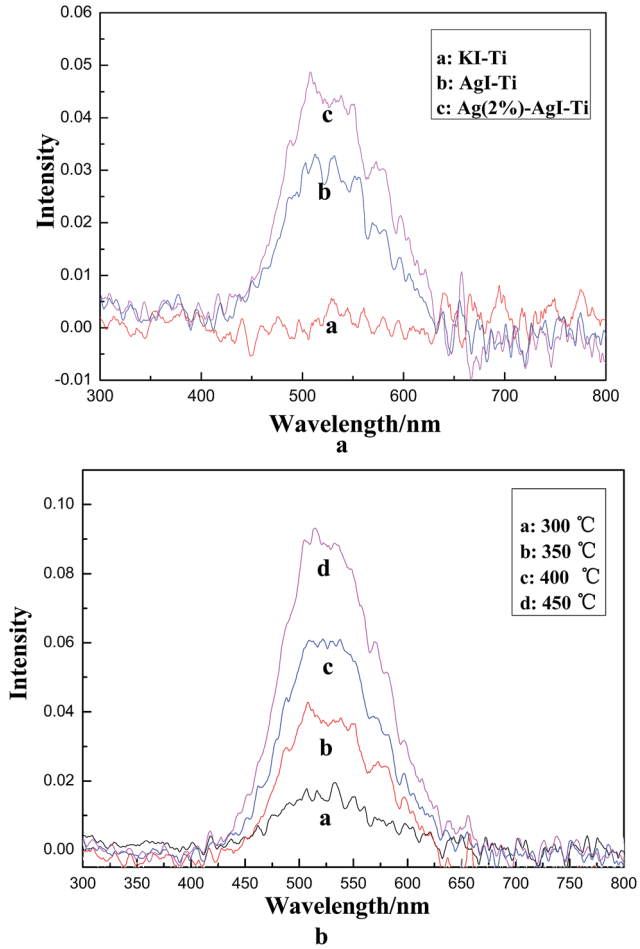

Fig. 9 The UV/vis spectroscopy analysis: the comparison of various catalysts (a), Ag(2%)–AgI–Ti at different temperatures (b).

until the concentration of HCl was 5000 ppm, and the results are shown in Fig. 9. Fig. 9(a) shows the comparison of the UV/vis spectra of various catalysts at 5000 ppm HCl. There was no characteristic peak for KI–Ti, while an absorption peak of 530 nm can be seen for AgI–Ti and Ag(2%)–AgI–Ti in Fig. 9(a), which was attributed to I_2. This result suggested that the iodine was formed by adding HCl, and Ag might have a catalytic effect on HCl. Active chlorine could be generated and then oxidize iodine ions to active iodine. Due to the high concentration of HCl, the amount of active iodine would be more, so that the reaction was readily able to generate I_2. The peak of I_2 of Ag(2%)–AgI–Ti was stronger than that of AgI–Ti, which might be due to the relatively high iodine content, indicating that having more silver nanoparticles could inhibit the decomposition of AgI.

The UV/vis spectra of Ag(2%)–AgI–Ti at different temperatures were shown in Fig. 9(b). The absorption peak intensity at 530 nm (I_2) increased with increasing temperature, suggesting that the yield of I_2 increased with increasing temperature. The amount of active Cl might increase with rising temperature, so that a greater amount of active I was generated, meaning that Hg^0 would be oxidized more effectively over the catalyst at high temperature.

The analysis of the ion chromatograms. To determine the reaction products, ion chromatography analysis was employed to analyze the oxidized mercury products, which were dissolved in ultrapure water. Fig. 10 shows the ion chromatogram of the reaction product. It can be seen from Fig. 10(b) that there was only one characteristic peak, which can be attributed to Cl^-, compared to the peak of the standard sample in Fig. 10(a). It was reported that iodine was more reactive than chlorine (by two magnitudes) for the removal of Hg^0,[19] while the peak of I^- was not found, indicting that the reaction product was not HgI_2. It may be that active I combined with Hg^0 in the formation of van der Waals intermediate molecules, such as Hg–I*, and then active chlorine converted the intermediate to $HgCl_2$, which was because chlorine was more competitive than iodine in bonding with the oxidized mercury due to its higher redox potential value.[31] In addition, active I would react with silver to generate AgI, maintaining the stability of iodine.

Based on the above results, the possible reaction paths for Hg^0 removal could be speculated as follows: HCl was adsorbed and activated by silver nanoparticles, and the generated Cl activated AgI to Ag···I*. Then, Ag···I* combined with Hg^0 in the form of Hg–I*, which reacted with adsorbed Cl on the surface of

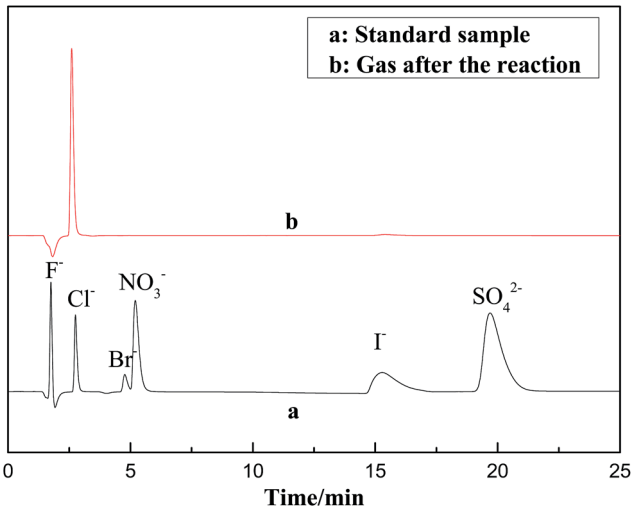

Fig. 10 The ion chromatograms of reaction product and standard sample.

the silver to generate $HgCl_2$ and AgI, maintaining the stability of the Ag(2%)–AgI–Ti catalyst.

The main reaction process for the Hg^0 oxidation over Ag(2%)–AgI–Ti can be seen in Fig. 11. As can be seen from Fig. 11, iodine in Ag(2%)–AgI–Ti mainly acted as an accelerant for Hg^0 oxidation by facilitating the formation of the intermediates. Then, chlorine can further convert the intermediate to the final product of $HgCl_2$. AgI was recycled in the reaction process, which was beneficial for Hg^0 oxidation over a long time.

Eqn (1)–(5) are some of the possible reactions during Hg^0 conversion:

$$4Ag\cdots HCl + O_2 \rightarrow 4Ag\cdots Cl^* + 2H_2O \quad (1)$$

$$AgI + Ag\cdots Cl^* \rightarrow Ag\cdots I^* + Ag\cdots Cl \quad (2)$$

$$Ag\cdots I^* + Hg^0 \rightarrow Ag + Hg\cdots I^* \quad (3)$$

$$Hg\cdots I^* + Ag\cdots Cl \rightarrow HgCl + AgI \quad (4)$$

$$HgCl + Cl^* \rightarrow HgCl_2 \quad (5)$$

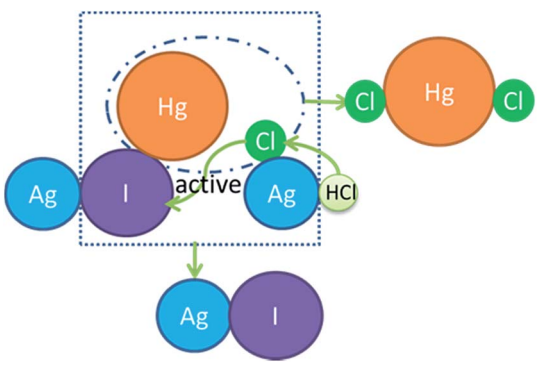

Fig. 11 The main reaction process for the Hg^0 oxidation over Ag(2%)–AgI–Ti.

The analysis of thermal stability. In order to study the thermal stability of the catalysts, thermogravimetric (TG) analysis was performed. Fig. 12 shows the TG curves of various catalysts. As can be seen from Fig. 12, the weights of AgI–Ti and Ag(2%)–AgI–Ti declined below 300 °C, which might be due to the surface adsorption of water. The weight of AgI–Ti was still declining slowly above 300 °C, indicating that some of the AgI might be decomposed to I_2 at high temperature. The weight of Ag(2%)–AgI–Ti was decreased little, demonstrating a very good stability at high temperature, and proving that Ag could efficiently inhibit the decomposition of AgI.

To verify the chemical stability of iodide, ion chromatography analysis was used to detect the change in the amount of iodide. The experimental process was as follows: a certain amount of Ag (2%)–AgI–Ti catalyst having reacted for 10 h and fresh catalyst were dissolved in sodium thiosulfate solution by ultrasonic dispersion for 24 h, and then the supernatant of the mixture was analyzed. Fig. 13 shows the ion chromatograms of Ag (2%)–AgI–Ti before and after reaction. The characteristic peak of iodine can be found in Fig. 13(a) and (b), demonstrating that iodine still existed on the surface of the catalyst. This revealed the stability of the iodine, and proved the conclusion above, in which iodine was an accelerant for Hg^0 oxidation by facilitating the formation of the intermediates. However, the amount of iodine decreased slightly, and the loss amount was about 20% after 10 h, which might be due to the fact that the active I on the surface of the catalyst was taken away due to the higher space velocity. Under actual conditions, the space velocity could be adjusted to reduce the loss of iodine, and iodine vapour could be also passed over the catalyst to recover the amount of iodine. Furthermore, the characteristic peak of chlorine was seen in Fig. 13. The peak intensity after reaction was stronger than that of the catalyst before reaction, proving that chlorine was adsorbed on the surface of the catalyst.

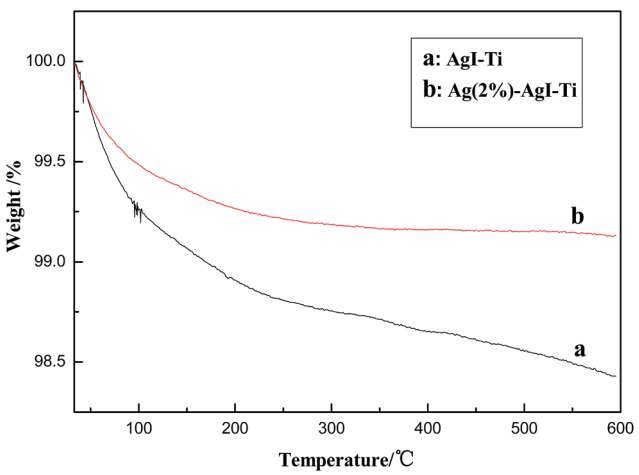

Fig. 12 The TG curves of various catalysts: AgI–Ti (a), Ag(2%)–AgI–Ti (b).

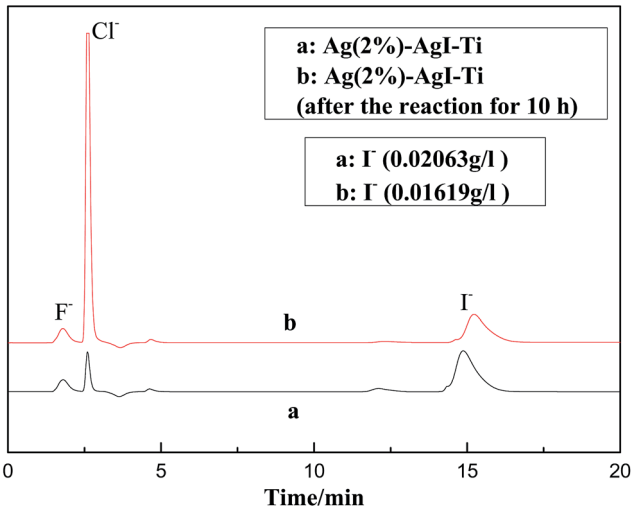

Fig. 13 The ion chromatograms of Ag(2%)–AgI–Ti before and after the reaction.

Conclusions

Ag(2%)–AgI–TiO_2 was an excellent and durable catalyst for Hg^0 catalytic oxidation, and could reach 100% with 5 ppm HCl at 350 °C, which was better than KI–Ti. Adding silver to AgI–TiO_2 can effectively prolong the time of high efficiency. A 2% Ag content was suitable, for which the Hg^0 oxidation efficiency was still above 90% after 10 h. AgI and Ag nanoparticles were loaded on the surface of TiO_2, and the addition of silver could inhibit the decomposition of AgI according to the analysis of physical and chemical characterization. The component analysis of Hg^0 oxidation indicated that HCl was the major oxidation component and O_2 was necessary; in addition, sulfur dioxide slightly inhibited the Hg^0 oxidization, while nitric oxide can promote the reaction, and water had little effect on the reaction. The reaction mechanism was probed by UV/vis spectroscopy and ion chromatography analysis; this indicated that HCl was adsorbed and activated by silver, and the generated Cl activated AgI to Ag···I*. Then, Ag···I* combined with Hg^0 in the form of Hg–I*, which reacted with adsorbed Cl on the surface of silver to generate $HgCl_2$ and AgI, maintaining the stability of the Ag(2%)–AgI–Ti catalyst. In addition, thermogravimetric (TG) analysis was performed, and proved that Ag(2%)–AgI–Ti displayed a good stability at high temperature. Furthermore, the ion chromatograms of Ag(2%)–AgI–Ti before and after the reaction revealed the chemical stability of AgI–Ti in the presence of Ag.

Acknowledgements

This study was supported by the Major State Basic Research Development Program of China (973 Program, no. 2013CB430005), the National Natural Science Foundation of China (no. 21277088, 50908145) and the National High-Tech R&D Program (863) of China (no. 2013AA065403, 2012AA062504).

References

1 Y. Zhao, R. L. Hao, P. Zhang and S. H. Zhou, *Fuel*, 2014, **136**, 113–121.
2 A. Suarez Negreira and J. Wilcox, *Energy Fuels*, 2015, **29**, 369–376.
3 S. S. Chen, H. C. Hsi, S. H. Nian and C. H. Chiu, *Appl. Catal., B*, 2014, **160**, 558–565.
4 J. K. Xie, Z. Qu, N. Q. Yan, S. J. Yang, W. M. Chen, L. G. Hu, W. J. Huang and P. Liu, *J. Hazard. Mater.*, 2013, **261**, 206–213.
5 H. Q. Yang, Z. H. Xu, M. H. Fan, A. E. Bland and R. R. Judkins, *J. Hazard. Mater.*, 2007, **146**, 1–11.
6 A. Beretta, N. Usberti, L. Lietti, P. Forzatti, M. Di Blasi, A. Morandi and C. La Marca, *Chem. Eng. J.*, 2014, **257**, 170–183.
7 S. J. Zhao, Y. P. Ma, Z. Qu, N. Q. Yan, Z. Li, J. K. Xie and W. M. Chen, *Catal. Sci. Technol.*, 2014, **4**, 4036–4044.
8 S. Aboud, E. Sasmaz and J. Wilcox, *Main Group Chem.*, 2008, **7**, 205–215.
9 F. Scala, *Environ. Sci. Technol.*, 2001, **35**, 4367–4372.
10 A. A. Presto and E. J. Granite, *Environ. Sci. Technol.*, 2006, **40**, 5601–5609.
11 E. Sasmaz, A. Kirchofer, A. D. Jew, A. Saha, D. Abram, T. F. Jaramillo and J. Wilcox, *Fuel*, 2012, **99**, 188–196.
12 J. Wilcox, E. Sasmaz, A. Kirchofer and S.-S. Lee, *J. Air Waste Manage. Assoc.*, 2011, **61**, 418–426.
13 Y. Chi, N. Q. Yan, Z. Qu, S. H. Qiao and J. P. Jia, *J. Hazard. Mater.*, 2009, **166**, 776–781.
14 S. H. Liu, N. Q. Yan, Z. R. Liu, Z. Qu, P. Wang, S. G. Chang and C. Miller, *Environ. Sci. Technol.*, 2007, **41**, 1405–1412.
15 Y. H. Yeom, M. J. Li, W. M. H. Sachtler and E. Weitz, *J. Catal.*, 2007, **246**, 413–427.
16 H. Xu, J. Yan, Y. G. Xu, Y. H. Song, H. M. Li, J. X. Xia, C. J. Huang and H. L. Wan, *Appl. Catal., B*, 2013, **129**, 182–193.
17 H. X. Shi, G. Y. Li, H. W. Sun, T. C. An, H. J. Zhao and P. K. Wong, *Appl. Catal., B*, 2014, **158**, 301–307.
18 C. Hu, X. X. Hu, L. S. Wang, J. H. Qu and A. M. Wang, *Environ. Sci. Technol.*, 2006, **40**, 7903–7907.
19 Z. Qu, N. Yan, P. Liu, J. Jia and S. Yang, *J. Hazard. Mater.*, 2010, **183**, 132–137.
20 N. Q. Yan, W. M. Chen, J. Chen, Z. Qu, Y. F. Guo, S. J. Yang and J. P. Jia, *Environ. Sci. Technol.*, 2011, **45**, 5725–5730.
21 Y. H. Zhang, Z. R. Tang, X. Z. Fu and Y. J. Xu, *Appl. Catal., B*, 2011, **106**, 445–452.
22 W. Sun, Y. Z. Li, W. Q. Shi, X. J. Zhao and P. F. Fang, *J. Mater. Chem.*, 2011, **21**, 9263–9270.
23 L. Dong, Y. He, T. Li, J. Cai, W. Hu, S. Wang, H. Lin, M. Luo, X. Yi, L. Zhao, W. Weng and H. Wan, *Appl. Catal., A*, 2014, **472**, 143–151.
24 J. Cao, Y. Zhao, H. Lin, B. Xu and S. Chen, *J. Solid State Chem.*, 2013, **206**, 38–44.
25 S. B. Atla, C.-C. Chen, C.-Y. Chen, P.-Y. Lin, W. Pan, K.-C. Cheng, Y. M. Huang, Y.-F. Chang and J.-S. Jean, *J. Photochem. Photobiol., A*, 2012, **236**, 1–8.

26 C. F. Almeida Alves, F. Oliveira, I. Carvalho, A. P. Piedade and S. Carvalho, *Mater. Sci. Eng., C*, 2014, **34**, 22–28.
27 P. M. Carrasco, M. Cortazar, E. Ochoteco, E. Calahorra and J. A. Pomposo, *Surf. Interface Anal.*, 2007, **39**, 26–32.
28 M. Bentley, M. Fan, B. Dutcher, M. Tang, M. D. Argyle, A. G. Russell, Y. Zhang, M. P. Sharma and S. M. Swapp, *J. Hazard. Mater.*, 2013, **262**, 642–648.
29 S. Tao, C. Li, X. Fan, G. Zeng, P. Lu, X. Zhang, Q. Wen, W. Zhao, D. Luo and C. Fan, *Chem. Eng. J.*, 2012, **210**, 547–556.
30 X. Ge and H.-L. Zhang, *J. Solid State Chem.*, 1998, **141**, 186–190.
31 Z. Qu, N. Q. Yan, P. Liu, Y. P. Chi and J. Jia, *Environ. Sci. Technol.*, 2009, **43**, 8610–8615.